

A PI polyamide–TPP conjugate targeting a mtDNA mutation induces cell death of cancer cells with the mutation

Nobuko Koshikawa¹ | Nanami Yasui¹ | Yuki Kida¹ | Yoshinao Shinozaki^{1,2} |
Kohei Tsuji¹ | Takayoshi Watanabe³ | Keizo Takenaga¹  | Hiroki Nagase¹ 

¹Division of Cancer Genetics, Chiba Cancer Center Research Institute, Chiba, Japan

²Organometallic Chemie Eduard-Zintl-Institut Technische Universität Darmstadt, Darmstadt, Germany

³Division of Innovative Cancer Therapeutics, Chiba Cancer Center Research Institute, Chiba, Japan

Correspondence

Hiroki Nagase, Laboratory of Cancer Genetics, Chiba Cancer Center Research Institute, 666-2 Nitona-cho, Chuoh-ku, Chiba 260-8717, Japan.
Email: hnagase@chiba-cc.jp

Funding information

The Mother and Child Health Foundation, Grant/Award Number: 28-7; Princess Takamatsu Cancer Research Fund; JSPS KAKENHI, Grant/Award Number: JP26290060, JP17H03602, JP16H01579 and JP20H03540; AMED, Grant/Award Number: 18ae0101051; The Tokyo Biochemical Research Foundation

Abstract

Mitochondrial DNA (mtDNA) mutations occur frequently in cancer cells, and some of them are often homoplasmic. Targeting such mtDNA mutations could be a new method for killing cancer cells with minimal impact on normal cells. Pyrrole-imidazole polyamides (PIPs) are cell-permeable minor groove binders that show sequence-specific binding to double-stranded DNA and inhibit the transcription of target genes. PIP conjugated with the lipophilic triphenylphosphonium (TPP) cation can be delivered to mitochondria without uptake into the nucleus. Here, we investigated the feasibility of the use of PIP-TPP to target a mtDNA mutation in order to kill cancer cells that harbor the mutation. We synthesized hairpin-type PIP-TPP targeting the A3243G mutation and examined its effects on the survival of HeLa cybrid cells with or without the mutation (HeLamA3243G cells or HeLamHeLa cells, respectively). A surface plasmon resonance assay demonstrated that PIP-TPP showed approximately 60-fold higher binding affinity for the mutant G-containing synthetic double-stranded DNA than for the wild-type A-containing DNA. When added to cells, it localized in mitochondria and induced mitochondrial reactive oxygen species production, extensive mitophagy, and apoptosis in HeLamA3243G cells, while only slightly exerting these effects in HeLamHeLa cells. These results suggest that PIP-TPPs targeting mtDNA mutations could be potential chemotherapeutic drugs to treat cancers without severe adverse effects.

KEYWORDS

apoptosis, mitochondria, mtDNA, mutation, pyrrole-imidazole polyamide

1 | INTRODUCTION

Human mitochondrial DNA (mtDNA) is a circular double-stranded DNA molecule of 16 569 bp that encodes 37 genes, including 22 tRNAs, 2 rRNAs and 13 structural genes critical for oxidative phosphorylation. Each cell contains 100–1000 copies of mtDNA.¹ It is well known that mtDNA is prone to somatic mutations due to a lack

of histones in the structure and a lack of effective repair mechanisms.¹ Such mutations play roles in aging, metabolic diseases, neurodegenerative diseases and neuromuscular disorders.² mtDNA mutations are also reported to be involved in cancer progression.³ We have recently reported that more than 70% of non-small cell lung carcinomas and colon carcinomas have nonsynonymous mutations in the NADH dehydrogenase (ND) genes and some of them are

This is an open access article under the terms of the Creative Commons Attribution-NonCommercial License, which permits use, distribution and reproduction in any medium, provided the original work is properly cited and is not used for commercial purposes.

© 2021 The Authors. *Cancer Science* published by John Wiley & Sons Australia, Ltd on behalf of Japanese Cancer Association.

significantly associated with metastasis.⁴ Of interest, we and others have reported that cancer-specific somatic mutations are often homoplasmic in a variety of cancers.^{4,5}

N-Methylpyrrole-N-methylimidazole polyamides (PIPs) bind to double-stranded DNA minor grooves via hydrogen bonds.^{6,7} They can be designed to bind to the sequences of genes of interest according to the numbers of hydrogen bonds in the nucleic acid bases⁸; pyrrole (Py) moieties and β -alanine (β) residues bind to A, T, and C nucleotides, and imidazole (Im) moieties bind to G nucleotides. Py/Py pairs recognize A/T or T/A base pairs, and Py/Im pairs recognize C/G base pairs. PIPs are cell-permeable and localize to the cell nucleus, where they inhibit the transcription of the genes. A striking feature of PIPs is that functional units such as the mitochondria-targeted cationic moiety and DNA-alkylating drugs, including 1-(chloromethyl)-5-hydroxy-1,2-dihydro-3H-benz[e]indole (seco-CBI), can be conjugated to the N- and C-termini.^{9,10} To date, several reports have demonstrated the anticancer effects of PIPs.^{11,12} We have also reported that DNA-alkylating PIPs targeting the mutant *KRAS* gene and *MYCN* gene amplification suppress tumor growth in colorectal cancer and high-risk neuroblastoma, respectively.¹³⁻¹⁵

mtDNA mutations seem to be ideal targets for PIPs in treating cancers because (a) mtDNA is essential for cell survival; (b) some cancer-specific mtDNA mutations are homoplasmic⁴; (c) mtDNA is more accessible for PIPs than nuclear DNA because of the lack of histones¹⁶; and (c) mtDNA is smaller in size than nuclear DNA, which may considerably reduce nonspecific binding of PIPs. Thus, we tried to assess the feasibility of the use of PIPs to target mtDNA mutations in order to treat cancer cells. We chose HeLa cybrid cells with wild-type mtDNA or the MELAS A3243G mutation in the *MT-TL1* (tRNA^{Leu(UUR)}) gene as experimental models because they have the same nuclear DNA; thus, only difference in mtDNA mutation status will be illuminated. The A3243G mutation has also been reported to be a somatic mutation in colon cancer, renal cell carcinoma, renal oncocytoma, and papillary thyroid carcinoma.¹⁷⁻²⁰ We tested here the effects of a hairpin-form pyrrole-imidazole polyamide-triphenylphosphonium (PIP-TPP) targeting the mutation. The results showed that PIP-TPP (CCC-018-TPP) significantly induced apoptosis in HeLa cybrid cells with mutant mtDNA but not in those with wild-type mtDNA.

2 | MATERIALS AND METHODS

2.1 | Cells and cell culture

HeLamHeLa (HeEB1) cells were established by reintroduction of HeLa mtDNA into mtDNA-less ρ^0 HeLa cells.^{21,22} HeLamA3243G cells were established by fusing ρ^0 HeLa cells with enucleated fibroblasts isolated from a person with the mtDNA A3243G mutation.²³ They were obtained from Prof. J.-I. Hayashi and Prof. K. Nakada (Tsukuba University) and cultured in Dulbecco's modified Eagle's medium (DMEM) supplemented with 0.01% pyruvate, 0.005% uridine, 1%

penicillin/streptomycin (Sigma-Aldrich), and 10% fetal bovine serum (FBS). Nontumorigenic human mammary epithelial MCF10A cells (PromoCell) were cultured in DMEM/F12 supplemented with 5% horse serum, 20 ng/mL epidermal growth factor (PeproTech), 0.5 μ g/mL hydrocortisone (Sigma-Aldrich), 100 ng/mL cholera toxin (Sigma-Aldrich), and 100 μ g/mL recombinant insulin (Humulin R, Eli Lilly Japan).

2.2 | Synthesis of PIP-TPP conjugate (CCC-018-TPP) targeting the mtDNA A3243G mutation

The PIP-TPP conjugate, CCC-018-TPP, was synthesized following a procedure of the solid-phase peptide synthesis with an assistance of a semiautomatic peptide synthesizer, PSSM-8 (Shimadzu) (Doc. S1). The purity of the product was determined to be >98% by liquid chromatography-mass spectrometry (LC-MS) as shown in Figure S2.

2.3 | Surface plasmon resonance (SPR) assay

The following biotin-conjugated mismatched tRNA^{Leu}-A and matched tRNA^{Leu}-G oligonucleotides were used: mismatched tRNA^{Leu}-A sequence, biotin-5'-GATGGCAGAGCCCGGTAATCGTTTTCGATTACCGGGCTCTGCCATC-3'; matched tRNA^{Leu}-G, biotin-5'-GATGGCAGGGCCCGGTAATCGTTTTTCGATTACCGGGCCCTGCATC-3' (the underlines show the sequences of interest). Each oligonucleotide was annealed and used for the biosensor-SPR assay. The kinetic measurements of the curves of polyamide binding to the biotin-labeled oligonucleotides and data processing were performed on a Biacore X100 system (GE HealthCare) as described previously.²⁴

2.4 | Droplet digital polymerase chain reaction (PCR) analysis

To determine the percentage of mtDNA A3243G in HeLamA3243G cybrid cells, droplet digital PCR was used. Total DNA was extracted from HeLamHeLa and HeLamA3243G cells using a DNeasy Blood & Tissue Kit (Qiagen). Digital PCR was performed with a QX200 Droplet Digital PCR System (Bio-Rad) using ddPCR MUT FAM and HEX assays (Bio-Rad, Cat# 10 049 047). The digital PCR mixture consisted of 8 μ L of nuclease-free H₂O, 10 μ L of 2x ddPCR SuperMix for Probes, 1 μ L of 20x target (FAM) and wild-type (HEX) primers/probes, and 1 μ L of sample DNA solution (10 ng) in a final volume of 20 μ L. After droplet generation with the Droplet Generator, thermal cycling was carried out using the following thermal profile: an initial step at 95°C for 10 minutes, 40 cycles of 94°C for 30 seconds and 55°C for 1 minute, one step of 98°C for 10 minutes, and a final step at 10°C. Data acquisition and analysis were performed using the Droplet Reader and QuantaSoft software, respectively.

2.5 | Assessment of PIP-TPP localization in mitochondria

Cells treated with 10 $\mu\text{mol/L}$ CCC-018-TPP for 24 hours were incubated with 50 nmol/L MitoTracker Red CMXRos (Thermo Fisher Scientific) for 5 minutes and fixed with 4% paraformaldehyde in phosphate-buffered saline (PBS) for 30 minutes at room temperature. After washing with PBS, the cells were treated with 0.5% Triton X-100 in PBS for 4 minutes for permeabilization. Blocking of nonspecific binding sites with 3% bovine serum albumin (BSA)/0.1% glycine/PBS was performed overnight at 4°C. The cells were then incubated with a rabbit polyclonal anti-TPP antibody (1:200 dilution, a gift from Prof. M. P. Murphy, Cambridge University, UK) in PBS for 1 hour. After washing with PBS, the cells were incubated with Oregon Green 488-conjugated goat anti-rabbit IgG (1:1000 dilution, Thermo Fisher Scientific) in PBS for 1 hour at room temperature. The cells were counterstained with 1 $\mu\text{g/mL}$ 4',6-diamidino-2-phenylindole (DAPI) and then mounted in VECTASHIELD Mounting Medium (Vector Laboratories, Inc). The samples were observed under a confocal laser scanning microscope (SP8, Leica Microsystems).

2.6 | Water soluble tetrazolium salts (WST) assay

Cells (3000 cells/well) were seeded in a 96-well plate 24 hours before the assay. They were then incubated with various concentrations of CCC-018-TPP for 48 or 72 hours. Dimethylsulfoxide (DMSO) was added to the control wells at 0.1%. Cell growth was measured with a Cell Counting Kit-8 (Dojindo) following the manufacturer's instructions.

2.7 | Reactive oxygen species (ROS) production assay

Cells were treated with vehicle alone or 10 $\mu\text{mol/L}$ CCC-018-TPP. The cells were washed once with serum-free DMEM, and then 25 nmol/L MitoSOX Red (Thermo Fisher Scientific) was added. After incubation for 15 minutes at 37°C, the cells were observed under a confocal laser scanning microscope.

2.8 | Assessment of mitophagy

Cells treated with vehicle alone or 10 $\mu\text{mol/L}$ CCC-018-TPP were fixed with 4% paraformaldehyde in PBS for 20 minutes, washed with PBS, and then permeabilized with 0.5% Triton X-100 in PBS for 4 minutes at room temperature. After washing with PBS, the cells were incubated with 3% BSA/0.1% glycine in PBS for 1 hour to block nonspecific binding sites. The cells were then incubated with a mouse monoclonal anti-cytochrome c antibody (1:100 dilution, Thermo Fisher Scientific) and a rabbit polyclonal anti-LC3 antibody (1:100 dilution, Cell Signaling Technology) for 1 hour at room temperature before being incubated with Alexa Fluor 647-conjugated

goat anti-mouse IgG (1:1000 dilution, Thermo Fisher Scientific) and Oregon Green 488-conjugated goat anti-rabbit IgG (1:1000 dilution, Thermo Fisher Scientific) for 1 hour at room temperature. After washing with PBS, the nuclei were stained with 1 $\mu\text{g/mL}$ DAPI, mounted in 1-4-diazabicyclo[2, 2, 2]-octane/polyvinyl alcohol (DABCO/PVA) mounting medium (Sigma-Aldrich) and observed under a confocal laser scanning microscope.

2.9 | Mitochondrial membrane potential (JC-1) assay

Cells seeded in the wells of a 96-well plate were treated with vehicle alone or 10 $\mu\text{mol/L}$ CCC-018-TPP for 48 hours. JC-1 assay reagent (10 μL) was added to each well, and the cells were incubated for 15 minutes at 37°C. Then, the cells were observed under a confocal laser scanning microscope. JC-1 is predominantly a monomer that yields green fluorescence in cells with low mitochondrial membrane potential, while the dye aggregates yield red to orange fluorescence in cells with high mitochondrial membrane potential.

2.10 | Assessment of fragmented nuclei

HeLamTHeLa and HeLamT A3243G cells were treated with vehicle alone or 10 $\mu\text{mol/L}$ CCC-018-TPP for 72 hours. The cells were fixed with 4% paraformaldehyde in PBS for 20 minutes, permeabilized with 0.1% Triton X-100 in PBS for 3 minutes and then stained with 1 $\mu\text{g/mL}$ DAPI. The cells were observed under a confocal laser scanning microscope, and the cells with fragmented nuclei were counted.

2.11 | Cleaved caspase-3 immunostaining

HeLamT A3243G cells were treated with vehicle alone or 10 $\mu\text{mol/L}$ CCC-018-TPP for 72 hours. The cells were fixed with 4% paraformaldehyde in PBS for 20 minutes, permeabilized with 0.1% Triton X-100 in PBS for 3 minutes, and then incubated with 3% BSA/0.1% glycine in PBS for 1 hour. They were then incubated with a rabbit polyclonal anti-cleaved caspase-3 (CC3) antibody (Cell Signaling Technology) followed by Alexa Fluor 488-conjugated goat anti-rabbit IgG. The cells were counterstained with 1 $\mu\text{g/mL}$ DAPI.

2.12 | Western blotting

Cells treated with CCC-018-TPP were lysed in radioimmunoprecipitation assay (RIPA) buffer containing Complete Protease Inhibitor Cocktail (Merck) and PhosSTOP (Merck Millipore). The lysates were centrifuged at 10 000 $\times g$ for 10 minutes at 4°C, and the supernatant was used for immunoblot analysis. Proteins were separated by 10% sodium dodecyl sulfate-polyacrylamide gel electrophoresis (SDS-PAGE) under reducing conditions and transferred to an Immobilon-P transfer membrane (Merck Millipore). The membrane was blocked

with BLOCK ACE (DS Pharma Biomedical Co., Ltd.) or 5% BSA in TBS-T (150 mmol/L NaCl, 20 mmol/L Tris-HCl, pH 7.5, 0.1% Tween 20). The primary antibodies used were a rabbit polyclonal anti-PARP-1 antibody (Cell Signaling Technology), a mouse monoclonal anti- γ -H2AX antibody (Cell Signaling Technology), and a mouse monoclonal anti- β -actin antibody (Santa Cruz Biotechnology). All primary antibodies were used at 1:1000 dilutions. The membrane was washed extensively with TBS-T and then incubated with the appropriate horse radish peroxidase (HRP)-conjugated secondary antibody (1:3000 dilution). ECL Plus Western Blotting Detection Reagent (Amersham Biosciences) was used for immunodetection. The membranes were scanned with a Luminoimaging Analyzer LAS4000 (GE Healthcare), and the bands were quantified via ImageJ software.

2.13 | Statistics

The data are presented as the mean \pm SD unless otherwise specified. Statistical significance was tested using one-way ANOVA and Tukey's test and evaluated against a predefined level of $P < .05$.

3 | RESULTS

3.1 | Specificity of CCC-018-TPP targeting A3243G

We designed and synthesized CCC-018-TPP that recognizes eight base pairs in the mtDNA sequence containing A3243G

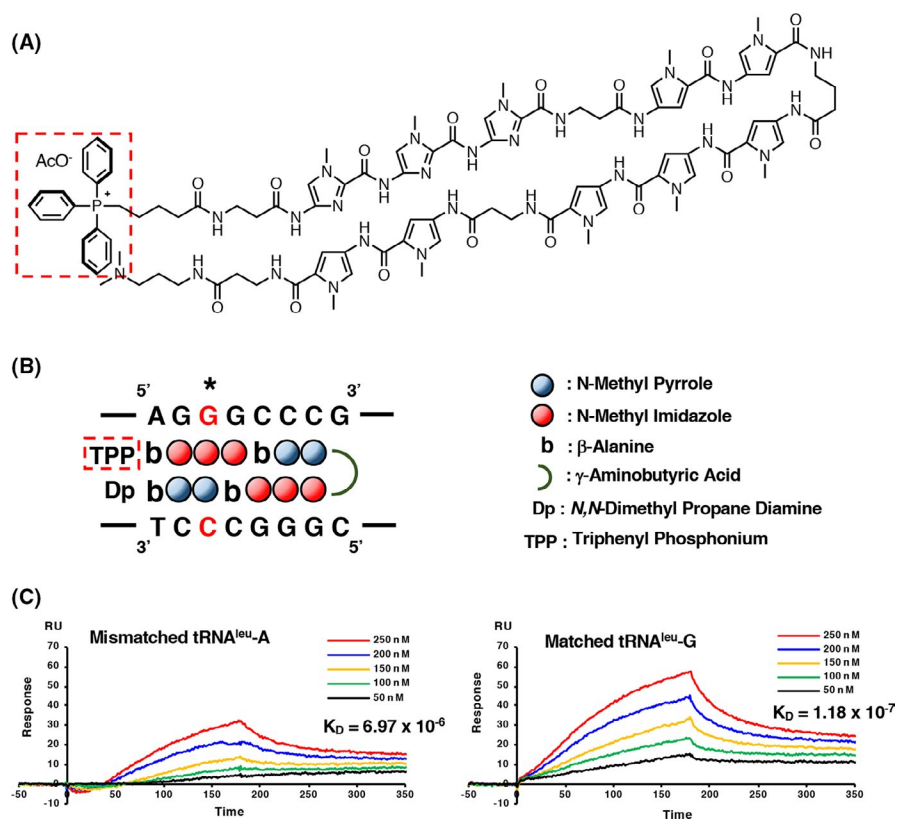
(Figure 1A,B, Figure S1). SPR assays demonstrated that the binding affinity of CCC-018-TPP for the hairpin oligonucleotide containing AGGGCCC (the matched sequence) was approximately 60 times higher than that for the oligonucleotide containing AGGACCC (the mismatched oligonucleotide) ($K_D \pm$ SE: $1.18 \times 10^{-7} \pm 0.5 \times 10^{-7}$ vs $6.97 \times 10^{-6} \pm 1.7 \times 10^{-6}$), demonstrating its efficacy in targeting the A3243G mutation (Figure 1C).

3.2 | Apoptosis-inducing activity of CCC-018-TPP in HeLamA3243G cells

HeLamA3243G cells contained approximately 99.8% mutant mtDNA, as determined by digital PCR (Figure S3). The mitochondria in the cells had a swollen, fragmented structure, which was quite different from the structure of the mitochondria in HeLamHeLa cells (Figure S4). When CCC-018-TPP was added to HeLamA3243G cells, it localized in mitochondria, as assessed by costaining with an anti-TPP antibody and MitoTracker Red (Figure 2A), although the mitochondrial membrane potential was probably low because the mutation is reported to reduce membrane potential.²⁵ Time-course experiments showed that CCC-018-TPP was retained for at least 5 days once incorporated in the mitochondria, but the amount of CCC-018-TPP gradually decreased (Figure S5). How CCC-018-TPP was metabolized remains unclear, but mitophagy, a mitochondrial quality control mechanism, could play a role in the degradation process as described below.

We then examined the effect of CCC-018-TPP on the survival of HeLamHeLa and HeLamA3243G cells. The WST assay showed that

FIGURE 1 Design and synthesis of the pyrrole-imidazole polyamide (PIP)-triphenylphosphonium (TPP). A, Chemical structure of CCC-018-TPP. The red dotted frame indicates TPP. B, Schematic drawing of the binding to double-stranded DNA containing A3243G. The asterisk indicated the position of 3243G. C, Binding affinity of CCC-018-TPP for mismatched (wild-type) and matched (mutant-type) oligonucleotides. The binding affinity was measured via surface plasmon resonance (SPR) assay. The blank-subtracted sensorgrams and K_D values are shown



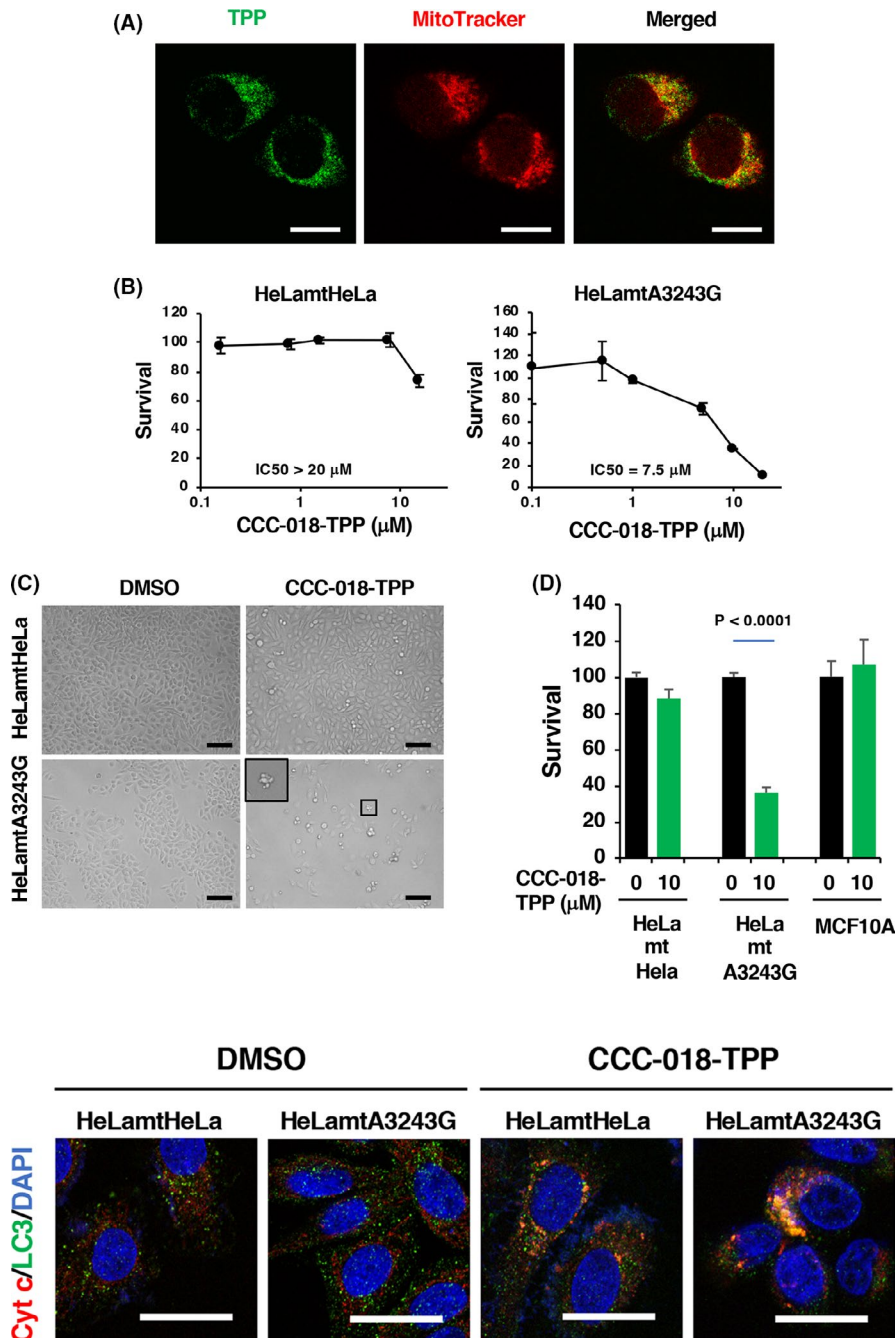


FIGURE 2 Cellular localization and cell death-inducing activity of CCC-018-TPP. A, Localization of CCC-018-TPP. HeLamtA3243G cells were treated with 10 $\mu\text{mol/L}$ CCC-018-TPP for 24 h and then incubated with MitoTracker Red for 5 min. Scale bars: 25 μm . B, Cell growth-inhibitory effect of CCC-018-TPP on HeLamtHeLa and HeLamtA3243G cells. The cybrid cells were treated with various concentrations of CCC-018-TPP for 48 h. C, Morphology of cybrid cells treated with DMSO or 10 $\mu\text{mol/L}$ CCC-018-TPP for 3 d. Scale bars: 200 μm . Cell growth was evaluated by WST assay. The data are presented as the mean \pm SD. D, Effect of CCC-018-TPP on the cybrid cells and MCF10A cells. Cell growth was evaluated by WST assay after treatment of the cells with 10 $\mu\text{mol/L}$ CCC-018-TPP for 72 h. The data are presented as the mean \pm SD

FIGURE 3 Induction of mitophagy by CCC-018-TPP. HeLamtHeLa and HeLamtA3243G cells were treated with 10 $\mu\text{mol/L}$ CCC-018-TPP for 52 h. The cells were stained for cytochrome c (Cyt c) and LC3 and then counterstained with DAPI. Scale bars: 40 μm

CCC-018-TPP significantly inhibited the growth of HeLamtA3243G cells in a dose-dependent manner but did not inhibit the growth of HeLamtHeLa cells at less than 10 $\mu\text{mol/L}$ (IC₁₀ and IC₅₀ for HeLamtHeLa and HeLamtA3243G cells were 10.0 $\mu\text{mol/L}$ and >20 $\mu\text{mol/L}$ and 1.5 $\mu\text{mol/L}$ and 7.5 $\mu\text{mol/L}$, respectively) (Figure 2B). Microscopic observation revealed that CCC-018-TPP induced cell death of HeLamtA3243G cells but not of HeLamtHeLa cells (Figure 2C). The cell death was characterized by apoptotic blebs²⁶ (Figure 2C, inset in bottom right panel). Because HeLamtHeLa and HeLamtA3243G cells have the same nuclear DNA, we concluded that the difference in sensitivity to CCC-018-TPP was due to the difference in mtDNA sequence. Importantly, CCC-018-TPP did not

affect the survival of normal epithelial MCF10A cells at 10 $\mu\text{mol/L}$, while that of HeLamtA3243G was significantly reduced (Figure 2D).

To determine the effects of CCC-018-TPP on mitochondrial integrity, we immunostained cells treated with vehicle alone or CCC-018-TPP for cytochrome c (Cyt c) and LC3. The results showed a marked increase in the number of cells with double-positive structures, which most likely represented autophagosomes containing mitochondria (indicating the occurrence of mitochondrial autophagy or mitophagy). (Figure 3). Time-course experiments demonstrated that the mitochondrial localization of CCC-018-TPP occurred as early as 1 hour after the addition. The localization was followed by enhancement of mtROS production by 3 hours, as detected by MitoSOX Red,

and by induction of mitophagy and nuclear fragmentation as early as 24 hours (Figure 4). The JC-1 assay showed that CCC-018-TPP treatment increased the number of green HeLamA3243G cells compared with HeLamHeLa cells, indicating decreased mitochondrial membrane potential (Figure 5A). We also examined the effects of CCC-018-TPP treatment on markers of the DNA damage response and apoptosis. Western blot analysis showed increases in γ -H2AX expression in HeLamA3243G cells as early as 3 hours after CCC-118-TPP treatment, but not in HeLamHeLa cells (Figure 5B,C). PARP-1 cleavage was also detected in CCC-018-treated HeLamA3243G cells (Figure 5C). CCC-018-TPP reproducibly increased full-length PARP-1 expression in HeLamHeLa cells, the reason for which is unknown. Furthermore, CCC-018-TPP increased the number of CC3-positive HeLamA3243G cells (Figure 5D). Thus, CCC-018-TPP induced nuclear DNA damage that was probably caused by ROS and apoptosis in HeLamA3243G cells.

4 | DISCUSSION

The present results demonstrated that CCC-018-TPP significantly inhibited cell growth and induced apoptosis of HeLamA3243G cells but only slightly induced apoptosis of HeLamHeLa cells. Because both HeLamA3243G and HeLamHeLa cells have the same nuclear DNA, these results indicate that this PIP-TPP conjugate exhibited its effects by targeting the A3243G mtDNA mutation.

Mitophagy is a process of mitochondrial quality control in which dysfunctional mitochondria are eliminated from a cell.²⁷ Because HeLamA3243G cells have an almost-homoplasmic A3243G mutation, their mitochondria must be nearly dysfunctional. However, as shown by coimmunostaining for cytochrome c and TPP, the level of mitophagy in HeLamA3243G cells was not very different from that in HeLamHeLa cells. However, CCC-018-TPP extensively induced mitophagy in HeLamA3243G cells, indicating that CCC-018-TPP affected some factors that can trigger mitophagy in the cells. One such factor may be mtROS. ROS play an important role in inducing autophagy in cells,^{28,29} although exactly how ROS regulate autophagy is unknown. Controlled mitophagy functions as a defense mechanism against mitochondrial dysfunction, but extensive mitophagy induces cell death. mtROS oxidize mitochondrial proteins and lipids and contribute to opening of the mitochondrial permeability transition pore (mPTP), from which cytochrome c is released; cytochrome c release in turn triggers the apoptotic pathway.³⁰ In fact, CCC-018-TPP induced the formation of plasma membrane blebs that were probably apoptotic bodies, further lowered mitochondrial membrane potential, increased the number of CC3-positive cells, and induced nuclear fragmentation. However, at present, it is unclear how CCC-018-TPP enhanced mtROS production. It has been reported that cell lines harboring the nearly homoplasmic A3243G mutation exhibit 70%–75% reductions in the levels of aminoacylated tRNA^{Leu}(UUR) and decreases in the mitochondrial protein synthesis rate.³¹ A3243G causes a respiratory defect mainly due to a deficiency of complex

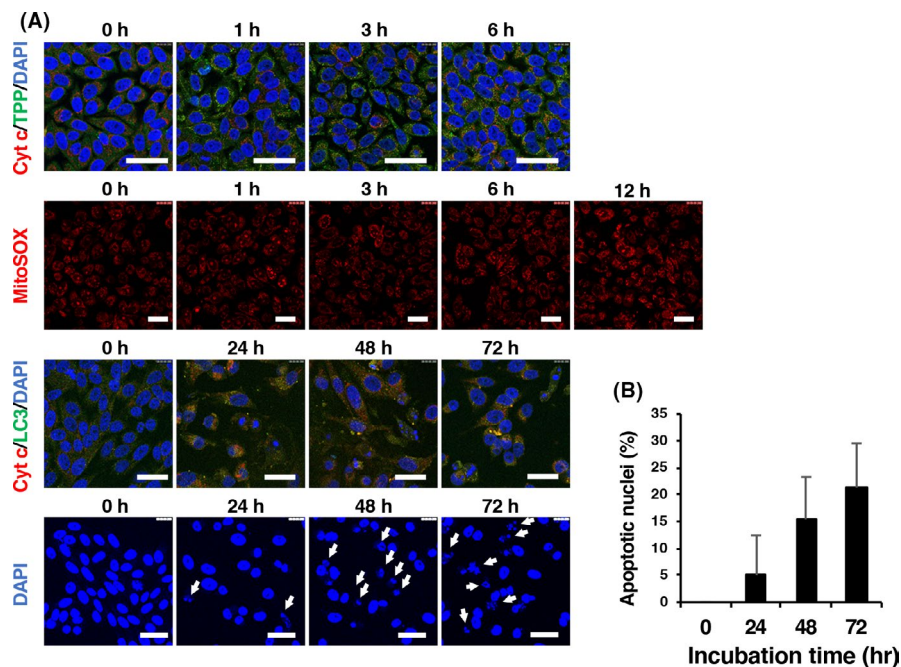


FIGURE 4 Time course of CCC-018-TPP uptake, mtROS production, mitophagy, and induction of nuclear fragmentation in HeLamA3243G cells. The cells were treated with 10 μ mol/L CCC-018-TPP for the times indicated. For detection of CCC-018-TPP uptake or mitophagy, cells were fixed and then immunostained for cytochrome c (Cyt c) and triphenylphosphonium (TPP) or Cyt c and LC3, respectively. For detection of mtROS production, cells were incubated with MitoSOX Red. For detection of fragmented nuclei, cells in glass-bottom culture dishes were fixed, permeabilized, and then incubated with DAPI. The percentage of the cells with fragmented nuclei was determined using confocal laser microscopy images ($n = 3, 5, 5,$ and 5 images for 0, 24, 48, and 72 h, respectively). The arrows indicate cells with fragmented nuclei. The data are presented as the mean \pm SD. Scale bars: 50 μ m

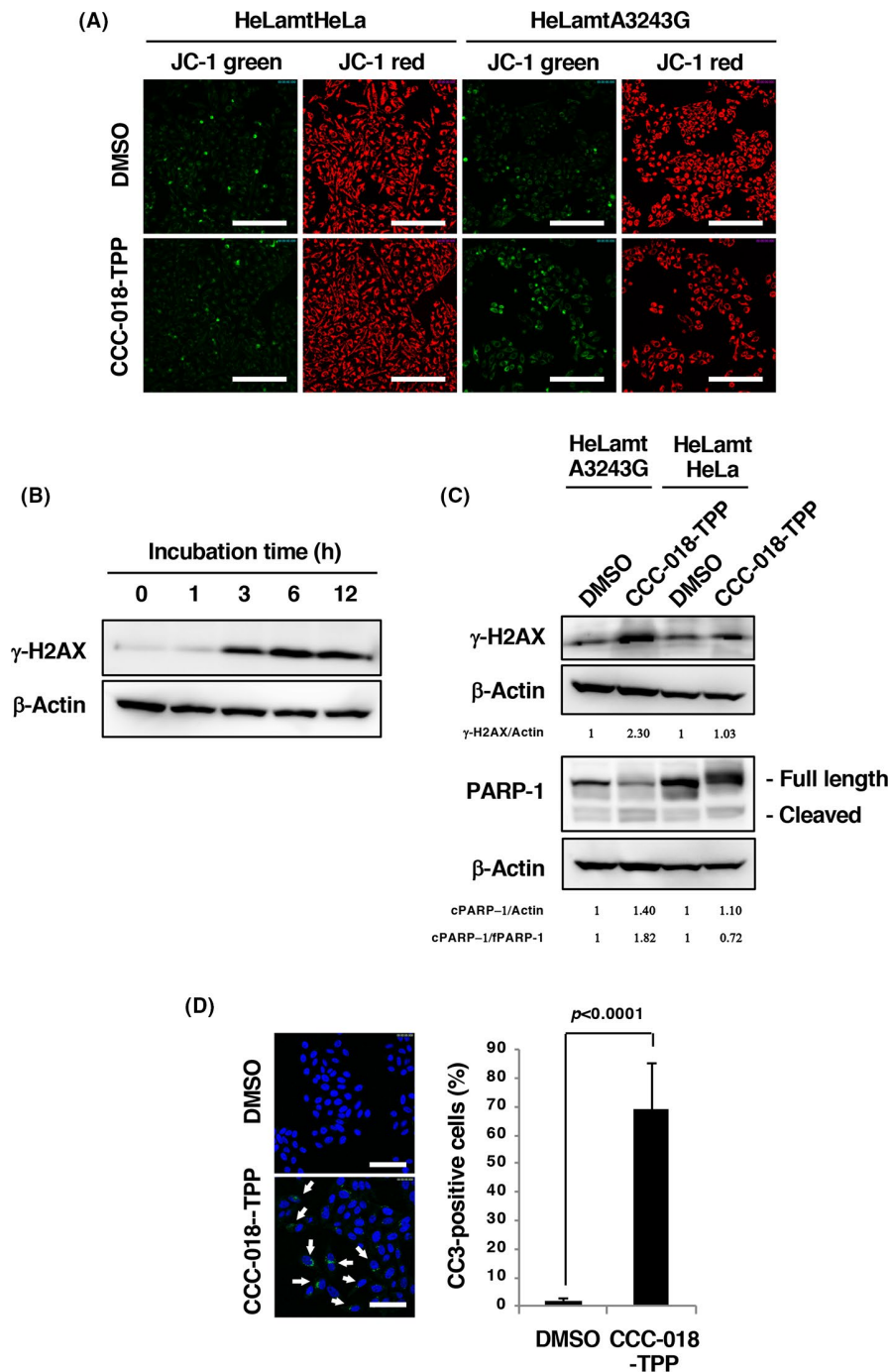


FIGURE 5 Apoptosis induction and expression of DNA damage- and apoptosis-related genes. A, JC-1 assay. HeLamHeLa and HeLamtA3243G cells were treated with 10 μ mol/L CCC-018-TPP for 48 h. Green and red fluorescence in cells indicate low and high mitochondrial membrane potential, respectively. Scale bars: 200 μ m. B, Time-course experiments of γ -H2AX expression after CCC-018-TPP treatment. HeLamtA3243G cells were treated with 20 μ mol/L CCC-018-TPP for the indicated times. C, Western blot analysis of γ -H2AX expression and PARP-1 cleavage. HeLamHeLa and HeLamtA3243G cells were treated with 20 μ mol/L CCC-018-TPP for 4 d. D, CC3 immunostaining. HeLamtA3243G cells were treated with 10 μ mol/L CCC-018-TPP for 3 d. After immunostaining for CC3, the cells were counterstained with DAPI and the percentage of CC3-positive cells was determined. The data are presented as the mean \pm SD. Scale bars: 50 μ m

I activity, a reduction in the O_2 consumption rate to 21%-46%, and a reduction in ATP synthase activity of up to 21%.²⁵ It also stimulates ROS production.^{32,33} These reports suggest that residual mitochondrial respiration was still occurring in HeLamtA3243G cells. It is possible that CCC-018-TPP might block mtDNA replication and/or tRNA^{Leu}(UUR) transcription in the cells and thereby further suppress respiratory chain function, causing mtROS overproduction, although this possibility should be examined in the future. The involvement of mtROS in an initial step may be supported by the time-course experiments, in which ROS overproduction was first observed after CCC-018-TPP entered mitochondria. The ROS overproduction was followed by mitophagy and apoptotic cell death. Generated

mitochondrial superoxide is converted to membrane-permeant hydrogen peroxide, which in turn may cross the nuclear membrane and damage nuclear DNA.³⁴ This may be the mechanism by which CCC-018-TPP increased γ -H2AX expression because time-course experiments showed that an increase in mtROS production was almost in parallel to that in γ -H2AX expression.

In summary, using cybrid cells harboring the MELAS A3243G mutation, which is also detected in neoplastic cells,¹⁷⁻²⁰ as a model, we showed, for the first time, the feasibility of the use of an mtDNA mutation-targeting PIP-TPP to kill cancer cells with the mutation. We and others have found many homoplasmic somatic mutations in mtDNA in human cancers and human cancer cell lines.^{4,35,36}

Therefore, discovery of cancer-specific mtDNA mutations in a patient followed by design and synthesis of a PIP-PPP targeting the mutations could be steps to advance precision cancer medicine. Further studies on the use of PIP-PPPs to target cancer-specific mutations are warranted in the future.

ACKNOWLEDGMENTS

We are grateful to Y. Kaihou and R. Igarashi, Division of Cancer Genetics, and Y. Nakamura, Laboratory of Oncogenomics, for technical assistance. This work was supported in part by the Princess Takamatsu Cancer Research Fund (to H. Nagase), JSPS KAKENHI (grant nos. JP26290060, JP17H03602, JP16H01579 and JP20H03540 to H. Nagase), AMED (grant no. 18ae0101051 to H. Nagase), The Tokyo Biochemical Research Foundation (to H. Nagase), and The Mother and Child Health Foundation (grant no. 28-7 to Y. Shinozaki).

DISCLOSURE

The authors have no conflicts of interest.

DATA AVAILABILITY STATEMENT

All data generated or analyzed are included in this published article (and its Supporting Information file Appendix S1).

ORCID

Keizo Takenaga  <https://orcid.org/0000-0002-5341-6742>

Hiroki Nagase  <https://orcid.org/0000-0002-3992-5399>

REFERENCES

- Gonçalves VF. Mitochondrial Genetics. *Adv Exp Med Biol.* 2019;1158:247-255. https://doi.org/10.1007/978-981-13-8367-0_13
- Lawless C, Greaves L, Reeve AK, Turnbull DM, Vincent AE. The rise and rise of mitochondrial DNA mutations. *Open Biol.* 2020;10:200061. <https://doi.org/10.1098/rsob.200061>
- Luo Y, Ma J, Lu W. The significance of mitochondrial dysfunction in cancer. *Int J Mol Sci.* 2020;21:E5598. <https://doi.org/10.3390/ijms21165598>
- Koshikawa N, Akimoto M, Hayashi JI, Nagase H, Takenaga K. Association of predicted pathogenic mutations in mitochondrial ND genes with distant metastasis in NSCLC and colon cancer. *Sci Rep.* 2017;7:15535. <https://doi.org/10.1038/s41598-017-15592-2>
- Nguyen NNY, Kim SS, Jo YH. Deregulated mitochondrial DNA in diseases. *DNA Cell Biol.* 2020;39:1385-1400. <https://doi.org/10.1089/dna.2019.5220>
- Dervan PB, Edelson BS. Recognition of the DNA minor groove by pyrrole-imidazole polyamides. *Curr Opin Struct Biol.* 2003;13:284-299. [https://doi.org/10.1016/s0959-440x\(03\)00081-2](https://doi.org/10.1016/s0959-440x(03)00081-2)
- Kawamoto Y, Bando T, Sugiyama H. Sequence-specific DNA binding Pyrrole-imidazole polyamides and their applications. *Bioorg Med Chem.* 2018;26(8):1393-1411. <https://doi.org/10.1016/j.bmc.2018.01.026>
- Urbach AR, Dervan PB toward rules for 1:1 polyamide:DNA recognition. *Proc Natl Acad Sci U S A.* 2001;98:4343-4348. <https://doi.org/10.1073/pnas.081070798>
- Zlelonka J, Slkora A, Hardy M, et al. Mitochondria-targeted triphenylphosphonium-based compounds: syntheses, mechanisms of action, and therapeutic and diagnostic applications. *Chem Rev.* 2017;117:10043-10120. <https://doi.org/10.1021/acs.chemrev.7b00042>
- Minoshima M, Bando T, Sasaki S, et al. DNA alkylation by pyrrole-imidazole seco-CBI conjugates with an indole linker: sequence-specific DNA alkylation with 10-base-pair recognition through heterodimer formation. *Am Chem Soc.* 2007;129:5384-5390. <https://doi.org/10.1021/ja065235a>
- Maeda R, Sato S, Obata S, et al. Molecular characteristics of DNA-alkylating PI polyamides targeting RUNX transcription factors. *J Am Chem Soc.* 2019;141:4257-4263. <https://doi.org/10.1021/jacs.8b08813>
- Liu K, Fang L, Sun H, et al. Targeting polo-like Kinase 1 by a novel pyrrole-imidazole polyamide-hoechst conjugate suppresses tumor growth in vivo. *Mol Cancer Ther.* 2018;17:988-1002. <https://doi.org/10.1158/1535-7163.MCT-17-0747>
- Hiraoka K, Inoue T, Taylor RD, et al. Inhibition of KRAS codon 12 mutants using a novel DNA-alkylating pyrrole-imidazole polyamide conjugate. *Nat Commun.* 2015;6:6706. <https://doi.org/10.1038/ncomms7706>
- Lin J, Hiraoka K, Watanabe T, et al. Identification of binding targets of a pyrrole-imidazole polyamide KR12 in the LS180 colorectal cancer genome. *PLoS One.* 2016;31(11):e0165581. <https://doi.org/10.1371/journal.pone.0165581>
- Yoda H, Inoue T, Shinozaki Y, et al. Direct targeting of MYCN gene amplification by site-specific DNA alkylation in neuroblastoma. *Cancer Res.* 2019;15(79):830-840. <https://doi.org/10.1158/0008-5472.CAN-18-1198>
- Onyango IG, Khan SM, Bennett JP Jr. Mitochondria in the pathophysiology of Alzheimer's and Parkinson's diseases. *Front Biosci (Landmark Ed).* 2017;22:854-872. <https://doi.org/10.2741/4521>
- Lorenc A, Bryk J, Golik P, et al. Homoplasmic MELAS A3243G mtDNA mutation in a colon cancer sample. *Mitochondrion.* 2003;3(2):119-124. [https://doi.org/10.1016/S1567-7249\(03\)00106-5](https://doi.org/10.1016/S1567-7249(03)00106-5)
- Meierhofer D, Mayr JA, Fink K, Schmeller N, Kofler B, Sperl W. Mitochondrial DNA mutations in renal cell carcinomas revealed no general impact on energy metabolism. *Br J Cancer.* 2006;94(2):268-274. <https://doi.org/10.1038/sj.bjc.6602929>
- Mayr JA, Meierhofer D, Zimmermann F, et al. Loss of complex I due to mitochondrial DNA mutations in renal oncocytoma. *Clin Cancer Res.* 2008;14(8):2270-2275. <https://doi.org/10.1158/1078-0432.CCR-07-4131>
- Xu B, Reznik E, Tuttle RM, et al. Outcome and molecular characteristics of non-invasive encapsulated follicular variant of papillary thyroid carcinoma with oncocytic features. *Endocrine.* 2019;64(1):97-108. <https://doi.org/10.1007/s12020-019-01848-6>
- Hayashi J-I, Ohta S, Kagawa Y, et al. Functional and morphological abnormalities of mitochondria in human cells containing mitochondrial DNA with pathogenic point mutations in tRNA genes. *J Biol Chem.* 1994;269(29):19060-19066.
- Hayashi J-I, Ohta S, Kikuchi A, Takemitsu M, Goto Y, Nonaka I. Introduction of disease-related mitochondrial DNA deletions into HeLa cells lacking mitochondrial DNA results in mitochondrial dysfunction. *Proc Natl Acad Sci U S A.* 1991;88:10614-10618.
- Hayashi J, Ohta S, Takai D, et al. Functional and morphological abnormalities of mitochondria in human cells containing mitochondrial DNA with pathogenic point mutations in tRNA genes. *J Biol Chem.* 1994;269:19060-19066. PMID: 75184.
- Kitagawa Y, Okumura K, Watanabe T, et al. Enrichment technique to allow early detection and monitor emergence of KRAS mutation in response to treatment. *Sci Rep.* 2019;9:11346. <https://doi.org/10.1038/s41598-019-47700-9>
- Matsubara M, Kanda H, Imamura H, et al. Analysis of mitochondrial function in human induced pluripotent stem cells from patients with mitochondrial diabetes due to the A3243G mutation. *Sci Rep.* 2018;8(1):949. <https://doi.org/10.1038/s41598-018-19264-7>

26. Aoki K, Satoi S, Harada S, Uchida S, Iwasa Y, Ikenouchi J. Coordinated changes in cell membrane and cytoplasm during maturation of apoptotic bleb. *Mol Biol Cell*. 2020;31(8):833-844. <https://doi.org/10.1091/mbc.E19-12-0691>
27. Yan X, Wang B, Hu Y, Wang S, Zhang X. Abnormal mitochondrial quality control in neurodegenerative diseases. *Front Cell Neurosci*. 2020;14:138. <https://doi.org/10.3389/fncel.2020.00138>
28. Schofield JH, Schafer ZT. Mitochondrial reactive oxygen species and mitophagy: a complex and nuanced relationship. *Antioxid Redox Signal*. 2021;34:517-530. <https://doi.org/10.1089/ars.2020.8058>
29. Fan P, Xie XH, Chen CH, et al. Molecular regulation mechanisms and interactions between reactive oxygen species and mitophagy. *DNA Cell Biol*. 2019;38:10-22. <https://doi.org/10.1089/dna.2018.4348>
30. Redza-Dutordoir M, Averill-Bates DA. Activation of apoptosis signalling pathways by reactive oxygen species. *Biochim Biophys Acta*. 2016;1863:2977-2992. <https://doi.org/10.1016/j.bbamcr.2016.09.012>
31. Park H, Davidson E, King MP. The pathogenic A3243G mutation in human mitochondrial tRNA^{Leu}(UUR) decreases the efficiency of aminoacylation. *Biochemistry*. 2003;42:958-964. <https://doi.org/10.1021/bi026882r>
32. Li J, Zhou K, Meng X, et al. Increased ROS generation and SOD activity in heteroplasmic tissues of transmitochondrial mice with A3243G mitochondrial DNA mutation. *Genet Mol Res*. 2008;7:1054-1062. <https://doi.org/10.4238/vol7-4gmr480>
33. Nissanka N, Moraes CT. Mitochondrial DNA damage and reactive oxygen species in neurodegenerative disease. *FEBS Lett*. 2018;592:728-742. <https://doi.org/10.1002/1873-3468.12956>
34. Munro D, Treberg JR. A radical shift in perspective: mitochondria as regulators of reactive oxygen species. *J Exp Biol*. 2017;220:1170-1180. <https://doi.org/10.1242/jeb.132142>
35. Schon EA, DiMauro S, Hirano M. Human mitochondrial DNA: roles of inherited and somatic mutations. *Nat Rev Genet*. 2012;13(12):878-890. <https://doi.org/10.1038/nrg3275>
36. Yu M. Somatic mitochondrial DNA mutations in human cancers. *Adv Clin Chem*. 2012;57:99-138. <https://doi.org/10.1016/b978-0-12-394384-2.00004-8>

SUPPORTING INFORMATION

Additional supporting information may be found online in the Supporting Information section.

How to cite this article: Koshikawa N, Yasui N, Kida Y, et al. A PI polyamide-TPP conjugate targeting a mtDNA mutation induces cell death of cancer cells with the mutation. *Cancer Sci*. 2021;112:2504-2512. <https://doi.org/10.1111/cas.14912>